scientific reports

Check for updates

OPEN

FTIR spectroscopic characterization reveals short-term macromolecular responses to photobiomodulation in mesenchymal stem cells

Ozlem Bozkurt-Girit✉ & Mahmut Alp Kilic

Photobiomodulation (low-level laser therapy) was reported to promote tissue repair, stem cell differentiation and proliferation; however, the underlying cellular mechanisms remain unclear. Investigating early, subtle cellular responses may be the key to optimize therapeutic outcomes and understand the biological effects of photobiomodulation. This study aimed to assess short-term macromolecular alterations in adipose-derived mesenchymal stem cells (ADSCs) subjected to 671 nm low-level laser irradiation via Fourier transform infrared (FTIR) spectroscopy. ADSCs were divided into control, 1-hour (1 H post-L) and 3-hour (3 H post-L) post-irradiation groups. 671 nm low-level laser irradiation was applied at a fluency of 25 J/cm^2. After 1 and 3 h, cells were collected and placed on the ATR unit of the FTIR spectrophotometer, dried under mild nitrogen flow and analyzed. Photobiomodulation resulted in explicit differences in FTIR spectra of 1 H and 3 H post-L groups, including alterations in lipid composition, protein secondary structure, protein phosphorylation together with changes in metabolic turnover of carbohydrates over time. Additionally, the membrane order decreased and fluidity increased in the 1 H post-L group, suggesting a temporary lateral phase separation in ADSC membranes. Photobiomodulation induced short-term structural and compositional alterations in biomolecules of ADSCs, which is further remarkable to provide insights into its action mechanism.

Keywords Adipose-derived mesenchymal stem cells, Photobiomodulation, Low-level laser therapy, Short-term effects, FTIR spectroscopy

Regenerative medicine is a multidisciplinary field of science that aims for the functional and physical renewal of organs and tissues, as well as the enhancement of their functions via therapeutic methods or applications, for the ultimate improvement of life quality of patients[1,2]. The identification of stem cells and the recognition of their therapeutic potential have brought a new direction to tissue engineering and regenerative medicine[3]; where the most frequently used cell type is mesenchymal stem cells.

One of the commonly used methods to increase regenerative capacity is photobiomodulation. The term photobiomodulation refers to biological changes in live cells, such as cellular activity or metabolism, in response to irradiation with a specific wavelength of light under certain conditions. Photobiomodulation, also referred to as low-level laser therapy (LLLT), is executed with the use of red and near-infrared lasers with a wavelength of 600–1100 nm at a low energy density (fluence) of 0.04–50 J/cm^2 in a continuous or pulsed mode[4,5]. This optical window enables a maximal tissue penetration with a minimum absorption of light by water[6]. Photobiomodulation was indicated to promote healing in injured cells and tissues, improve regenerative capacity[7], modulate cell metabolism[8], enhance cell migration during gingival wound healing[9], reduce inflammation and accelerate wound healing in diabetic patients[10]. Moreover, it was also reported to increase cell viability and proliferation[11], modulate inflammation[12], reduce apoptosis and support cell migration, which may play a key role in tissue repair[13] in mesenchymal stem cells. Although efforts are being made, the exact molecular mechanisms of photobiomodulation could not be explained in detail yet. Unlike pharmaceutical agents, the effects of low-level laser irradiation on cells depend on parameters such as the laser's wavelength and applied energy density as well as the type of the irradiated cell[11,14]. Studies reported that photobiomodulation via usage of 600 to 700 nm wavelengths stimulate proliferation and increase the differentiation of mesenchymal stem

Department of Biophysics School of Medicine, Aydın Adnan Menderes University, Aydın 09010, Turkey. ✉email: ozlem.bozkurt@adu.edu.tr

cells[11]. Within this wavelength range, Moore et al.[15] have demonstrated that the most efficient cell proliferation response of mouse vascular endothelial cells and fibroblasts were observed in 665 to 675 nm. The use of red and infrared light in photobiomodulation was reported to exert a biphasic dose response, where low energy density (fluence) results in weak responses at the cellular level, the increase in energy density results in beneficial effects and high fluence may disrupt cell proliferation and even induce apoptosis[16,17]. For example, low-level laser irradiation at low fluence increases tumor growth factor expression, while higher fluencies tend to suppress it[18,19]. Therefore, assessing dose-dependent effects of photobiomodulation is crucial. In addition, increased cell metabolism and proliferation were observed in both normal and cancer cell lines after photobiomodulation. Consequently, a better understanding of the cellular processes is pivotal for determining probable outcomes of photobiomodulation or for the design of efficient treatment protocols.

Recent scientific advancements highlight that cellular processes, stemming from molecular functioning, are deeply interconnected and largely reliant on the structural and dynamic properties of biomolecules[20]. Pathological conditions or therapeutic interventions can significantly alter the molecular structure, composition, and dynamics of tissues, cells, and membranes. Therefore, understanding the relationships between structure and function is essential for recognizing disease pathophysiology and the mechanisms of therapeutic actions. Fourier transform infrared (FTIR) spectroscopy is a fast, reliable, and increasingly valuable tool for examining the structural and dynamic properties of biomolecules in various samples. The recent increase in its application underscores its effectiveness in accurately interpreting cellular functions and metabolic processes[21–33]. FTIR spectroscopy was previously used to analyze the effect of Er-YAG laser on human dentin[34] and on rat bone slices together with human enamel and dentin[35]. As far as is known, FTIR spectroscopy was previously used to characterize molecular and biochemical alterations following photobiomodulation on snake venom intoxicated muscles[36] and MCF-7 breast cancer cells[37]. Magrini et al.[37] have reported that light can influence cell metabolism of MCF-7 cancer cells depending on the laser fluence.

This study aims to evaluate the initial biophysical response of adipose-derived mesenchymal stem cells (ADSCs) when exposed to photobiomodulation, a 671 nm low-level laser irradiation at a fluence of 25 J/cm², by the use of FTIR spectroscopy. The use of 671 nm was selected as this wavelength falls within the effective photobiomodulation range for ADSCs, providing an optimal tissue penetration and mitochondrial activation. As far as is known, this current study provides the first detailed FTIR-based spectral characterization of biomolecular responses in ADSCs following photobiomodulation. The structural, compositional and dynamic response in ADSCs at 1-hour and 3-hour post low-level laser exposure was reported for the first time in this current study. Our findings indicated ongoing differences over time in lipid composition and structure, protein structure and phosphorylation, metabolic turnover, membrane order and fluidity in ADSCs exposed to 671 nm low-level laser. The herein reported short-term structural and compositional responses to photobiomodulation might provide new insights into the mechanism of low-level laser action at cellular level and have implications for the design of future therapeutic applications in regenerative medicine.

Results

Cell proliferation and Hsp70 protein expression levels

Figure 1a shows a summary of the applied experimental procedures in the study and Fig. 1b demonstrates the experimental setup for laser irradiation. After the isolation and characterization of ADSCs, the cells were exposed to 671 nm laser with energy densities of 0 (control), 1, 5, 10, 25 and 50 J/cm^2 and cell viability of the irradiated cells were determined via MTT test (Fig. 1c). Cell viability was significantly improved following laser irradiation at fluencies of 25 and 50 J/cm^2, with the most notable effect seen at 50 J/cm^2. Although the dose of 50 J/cm^2 resulted in a more pronounced increase in cell viability in initial tests, the exposure time required for this dose -due to the single-channel laser system and sequential well illumination - was twice than that of 25 J/cm^2. Consequently, the usage of 50 J/cm^2 could significantly prolong the total experiment time and thereby could introduce variability in incubation conditions across wells. In order to maintain consistency, minimize time-based artifacts, and ensure compatibility with live-cell analyses, we proceeded with 25 J/cm^2 as the highest practical dose for detailed investigation. This decision effectively limited the irradiation time to around 3 min per well for subsequent experiments to reduce environmental stress and maintain cell viability.

Figure 1d demonstrates the Western blot images of Hsp70 and GAPDH proteins and Fig. 1e shows the fold change in Hsp70 protein expression levels compared to that of GAPDH in ADSCs after exposure to 25 J/cm² laser irradiation. The corresponding full-length blots are presented in the Supplementary Figure S1. The Hsp70 protein expression levels were decreased in 1 H post-L and increased in 3 H post-L groups, but the alterations were not statistically significant.

FTIR spectral characterization

Figure 2 demonstrates the representative FTIR spectra of control, 1 H and 3 H post-L groups in 4000–850 cm^{-1} (a), 3050–2800 cm^{-1} (b), 1800–800 cm^{-1} (c) and 1200–850 cm^{-1} (d) spectral regions. The assignments of the labelled spectral bands in Fig. 2 were given in Table 1. The alterations in the frequencies, band areas and bandwidths of some of the spectral bands were represented in Table 2. The shift in frequency of a spectral band give information on the structural alterations in the related function group, whereas the intensities and/or the area under spectral bands give relative concentrations of the related functional groups according to Beer-Lambert's law[33]. In order to eliminate potential experimental misrepresentation, band area ratios were used for a more precise comparison of the effects of low-level laser irradiation on AD-MSCs. The calculated band area ratios and their interpretation were given in Table 3, and the results were represented in Fig. 3. FTIR spectra of 1 H and 3 H post-L groups displayed apparent differences in most of the spectral bands. In order for a more explicable representation, the results of spectral characterization were organized in three subsections as lipids, proteins and protein structure, nucleic acids and carbohydrates.

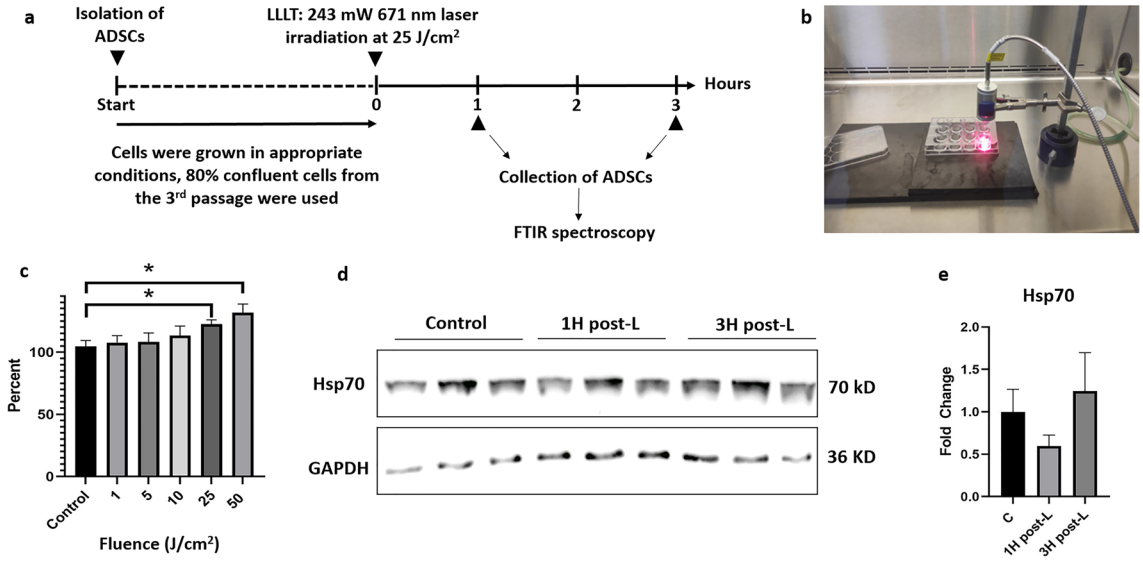

Fig. 1. (a) The schematic diagram of the timeline of the applied procedures. (b) The experimental setup for laser irradiation to the ADSCs. (c) the results of the MTT test demonstrating the changes in cell viability upon laser exposure at different energy densities of 0 (control), 1, 5, 10, 25 and 50 J/cm^2. (d) Western blot images of Hsp70 and GAPDH protein levels and (e) the fold change in Hsp70 protein expression levels compared to that of GAPDH in ADSCs of control, 1 H post-L and 3 H post-L groups. The full-length Western blots used for calculation are presented in Supplementary Figure S1. The data of MTT test and Hsp70 protein expression levels were compared by the use of one-way ANOVA with Dunn's test as a post-hoc test. The degree of significance was denoted as $^*p < 0.05$. The analysis of Hsp70 protein expression levels revealed non-significant alterations in between the groups.

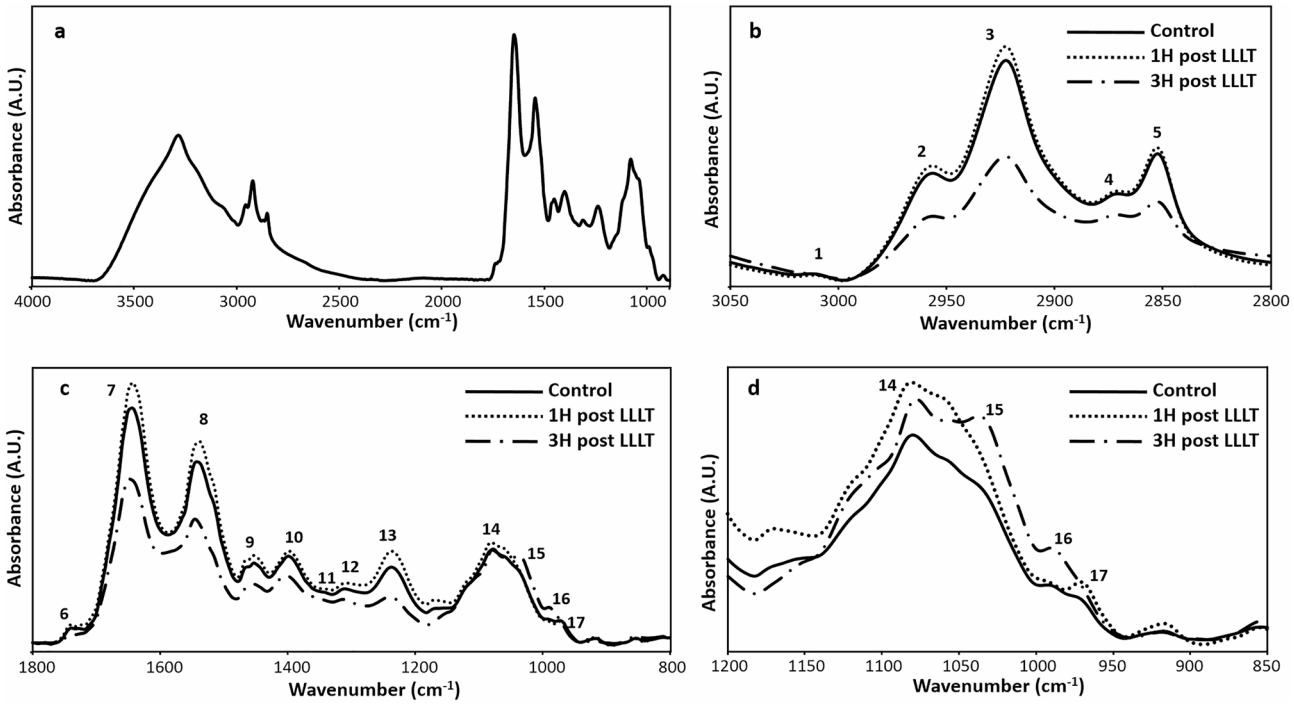

Fig. 2. (a) The representative FTIR spectra of control ADSCs in 4000–850 cm^{-1} region, the representative FTIR spectra of control, 1 H post-L and 3 H post-L groups (b) in 3050–2800 cm^{-1}, (c) in 1800–800 cm^{-1}, (d) in 1200–850 cm^{-1} region. Spectra were baseline corrected and normalized with respect to Amide A band located at 3282 cm^{-1} for visual demonstration.

Band No	Wavenumber (cm^{-1})	Definition
1	3010	Olefinic ν(HC = CH) of unsaturated fatty acids [26, 27, 32, 33, 38]
2	2957	$\nu_{as}(CH_3)$: equal contribution from lipids and proteins [26, 32, 33, 38, 39, 40]
3	2923	$\nu_{as}(CH_2)$: mainly lipids [26, 27, 28, 30, 32, 33, 38, 39, 40]
4	2873	$\nu_{s}(CH_3)$: mainly proteins [26, 27, 28, 32, 33, 38, 39]
5	2852	$\nu_{s}(CH_2)$: mainly lipids [26, 27, 28, 30, 32, 33, 38, 39, 40]
6	1740	ν(C = O) carbonyl ester of lipids, cholesterol esters, triglycerides [28, 30, 32, 33, 38, 39, 40, 41, 42]
7	1643	Amid I of proteins, %80 ν(C = O), %10 δ(N-H), %10 ν(C-N) vibrations [27, 28, 30, 32, 33, 39]
8	1542	Amid II of proteins, %60 δ(N-H), %40 ν(C-N) vibrations [27, 28, 30, 32, 33, 39]
9	1453	$\delta(CH_2)$ of lipids [26, 27, 28, 39, 41]
10	1399	$\nu_{s}(COO^{-})$ of fatty acids and protein side chains [28, 33, 39]
11	1340	CH_2 side chain vibrations of collagen [21, 26, 29, 37]
12	1311	Amide III: proteins, 40% δ(N-H), 40% ν(C-N), 20% ν(C-C) vibrations [28, 33, 41]
13	1236	$\nu_{as}(PO_2^{-})$ of phospholipids and nucleic acids [24, 28, 32, 33, 39]
14	1079	$\nu_{s}(PO_2^{-})$ of nucleic acids and phospholipids [21, 24, 28, 32, 33, 39]
15	1035	ν(C–O) of carbohydrates, glucose [26, 28, 33]
16	990	RNA backbone vibrations [33, 41, 40, 42]
17	970	$\nu_{s}(PO_4^{-2})$ stretching mode of dianionic phosphate monoesters of phosphorylated proteins or nucleic acids [23, 38, 40, 41]

Table 1. The assignments of the spectral bands labelled in Fig. 2. as, antisymmetric; s, symmetric; ν, stretching; δ, bending.

Band No	Wavenumber (cm^{-1})	Control	1 H post-L	3 H post-L
Band Frequency				
1	3010	3010.86 ± 0.38	$3009.64 \pm 0.17^{*}$	$3011.03 \pm 0.29^{‡}$
3	2923	2923.48 ± 0.12	$2922.70 \pm 0.25^{*}$	$2923.80 \pm 0.12^{‡‡‡}$
5	2852	2852.89 ± 0.07	2852.49 ± 0.19	$2853.17 \pm 0.08^{‡‡}$
7	1643	1643.90 ± 0.54	$1641.31 \pm 0.34^{**}$	$1646.16 \pm 0.36^{**, ‡‡‡}$
8	1542	1542.24 ± 1.03	$1537.99 \pm 0.45^{**}$	$1545.60 \pm 0.46^{*, ‡‡‡}$
Bandwidth				
3	2923	10.25 ± 0.07	$11.94 \pm 0.11^{***}$	$11.81 \pm 0.09^{***}$
5	2852	5.53 ± 0.14	5.96 ± 0.10	$5.11 \pm 0.16^{‡‡}$
Band area				
1	3010	1.24 ± 0.06	1.05 ± 0.16	$1.54 \pm 0.13^{‡}$
6	1740	0.42 ± 0.04	0.42 ± 0.11	0.27 ± 0.03
7	1643	13.12 ± 0.83	15.12 ± 2.17	$8.60 \pm 0.71^{‡}$
8	1542	10.45 ± 0.80	12.38 ± 1.64	$7.27 \pm 0.62^{‡}$
15	1035	2.30 ± 0.15	1.89 ± 0.26	$3.16 \pm 0.33^{‡‡}$
16	990	0.83 ± 0.07	0.83 ± 0.13	$1.28 \pm 0.13^{*,‡}$

Table 2. Changes in the frequency, band area and bandwidth values of some absorption bands in the FTIR spectra of ADSCs in control, 1 H post-L and 3 H post-L groups. The data were represented as mean ± standard error of mean. Comparison was performed by the one-way ANOVA test with Tukey's as a post-hoc test. A p value equal or less than 0.05 was considered as statistically significant ($^{*}p < 0.05$, $^{**}p < 0.01$, $^{***}p < 0.001$). The degree of significance was denoted by * for the comparison of control with the other groups, by ‡ for the comparison of 1 H post-L group with 3 H post-L group.

Lipids

The olefinic band located around 3010 cm^{-1} can be used to monitor unsaturated lipids, whereas the CH_2 antisymmetric and symmetric stretching bands located at 2923 and 2852 cm^{-1}, respectively, are used to monitor saturated lipids[26,27,32,33,38]. The area of olefinic band was observed to be slightly decreased in 1 H post-L group and significantly increased in 3 H post-L group in comparison to 1 H post-L group ($p < 0.05$, Table 2). In order to obtain a more precise result, unsaturated lipid content ($A_{3010}/A_{2957+2923+2852+1453}$) and unsaturated/saturated lipid content ($A_{3010}/A_{2923+2852}$) were calculated[26,27,33] (Table 3). The unsaturated lipid content, which demonstrate the content of double bonds in lipids, and the unsaturated/saturated lipid ratio were both observed to be decreased in 1 H post-L group ($p < 0.001$) and to be increased in 3 H post-L group ($p < 0.001$, Fig. 3a, b). Moreover, the alterations in the carbonyl group amount in lipids (band area ratio $A_{1740}/A_{2923+2852}$)[26,32], aliphatic chain length

Area Ratio	Biomolecular Origin	Indication
$A_{3010}/A_{2957+2923+2852+1453}$	ν(Olefinic = CH)/Total lipid	Unsaturated lipid content
$A_{3010}/A_{2923+2852}$	ν(Olefinic = CH)/$\nu_{as}(CH_2)$+ $\nu_s(CH_2)$	Unsaturated/saturated lipids
$A_{1740}/A_{2923+2852}$	ν(C = O)/$\nu_{as}(CH_2)$ + $\nu_s(CH_2)$	Carbonyl group amount in lipids
A_{2923}/A_{2957}	$\nu_{as}(CH_2)/\nu_{as}(CH_3)$	Aliphatic chain length
$A_{2923+2852}/A_{1643+1542}$	$\nu_{as}(CH_2)$ + $\nu_s(CH_2)$/Amide I + amide II	Lipid/protein
$A_{1643}/A_{1643+1542}$	Amide I/Amide I + Amide II	Protein concentration
A_{1236}/A_{2957}	$\nu_{as}(PO_2^-)/\nu_{as}(CH_3)$	Protein phosphorylation
A_{1542}/A_{1340}	Amide II/A_{1340}	Collagen integrity
$A_{990}/A_{1236+1079}$	ν(C-O), δ(C-N-C)/$\nu_{as}(PO_2^-)$ + $\nu_s(PO_2^-)$	RNA/PO_2^- antisym. + sym. stretching
$A_{1236+1079}/A_{1643+1542}$	$\nu_{as}(PO_2^-)$ + $\nu_s(PO_2^-)$/Amide I + amide II	PO_2^- antisym. + sym. stretching/protein
$A_{1035}/A_{1643+1542}$	ν(C–O) of carbohydrates/Amide I + Amide II	Glucose/protein
A_{1035}/A_{1079}	ν(C–O) of carbohydrates/$\nu_s(PO_2^-)$	Metabolic turnover

Table 3. The calculated area ratios of the IR bands, their biomolecular origins and indications. as, antisymmetric; s, symmetric; ν, stretching.

(band area ratio A_{2923}/A_{2957})[30] were monitored by the use of relevant band areas (Table 3). The carbonyl amount in lipids and lipid aliphatic chain length were both observed to be significantly decreased in 3 H post-L group ($p < 0.05$) in comparison to 1 H post-L group (Fig. 3c and d). These findings indicated that following laser irradiation, lipid composition and distribution were altered differently at 1-hour and 3-hour post-irradiation.

The frequency shifts and alterations in bandwidth of the CH_2 antisymmetric stretching band give information on the lipid order and lipid dynamics of the system, respectively[21,27,33]. The wavenumber (band location) of the CH_2 antisymmetric stretching band shifted to lower values ($p < 0.05$) in 1 H post-L group indicating an increase in the order of the system[21]. Whereas in the 3 H post-L group, the wavenumber of this band shifted to higher values ($p < 0.001$) compared to 1 H post-L group (Table 2), indicating a decrease in the order. The bandwidth of the CH_2 antisymmetric stretching band was observed to be increased in both laser irradiated groups in comparison to control ($p < 0.001$, Table 2), indicating an increase in lipid dynamics, i.e. fluidity[21,33].

Proteins and protein structure

Amide I and II are the main protein bands in an FTIR spectrum, and the band areas of amide I and amide II bands were both observed to be slightly increased in 1 H post-L group and significantly decreased in 3 H post-L group ($p < 0.05$, Table 2). Since band area ratios yield a more reliable comparison of the groups, the amide I/amide I + II ($A_{1643}/A_{1643+1542}$) ratio[32,33] (Table 3) was calculated monitor the alteration in protein concentration of ADSCs. This ratio revealed that total protein content was not altered in control and laser irradiated groups (Fig. 3f). Lipid to protein ratio ($A_{2923+2852}/A_{1643+1542}$)[32,33] was slightly decreased in 1 H post-L group, but was significantly increased in 3 H post-L group ($p < 0.001$, Fig. 3e). These data suggested that lipid content was significantly increased in 3 H post-L group, as protein concentration remained unchanged.

However, there were significant alterations in protein structure as revealed by FTIR spectral characterization. Firstly, the band located at 970 cm^{-1}, which was attributed to the PO_4^{-2} symmetric stretching mode of dianionic phosphate monoesters of phosphorylated proteins or nucleic acids[23,38–40], was prominently notable in 1 H post-L group, when compared to 3 H post-L group (Fig. 2d) in the FTIR spectra. In order to obtain a more precise information, band area ratio of the PO_2^- antisymmetric stretching to the CH_3 antisymmetric stretching (A_{1236}/A_{2957}) was calculated (Table 3) to comment on the level of protein phosphorylation in the ADSCs[22,32,33]. Protein phosphorylation was observed to be significantly increased in 1 H post-L group in comparison to control ($p < 0.05$), and significantly decreased in 3 H post-L group in comparison to both control ($p < 0.01$) and 1 H post-L group ($p < 0.001$) (Fig. 3g).

As laser irradiation was suggested to stimulate collagen production[41], the influence of photobiomodulation on quality of collagen in ADSCs were monitored by the band area ratio A_{1542}/A_{1340} (Table 3) calculated by dividing the area of amide II band to that of the band located at 1340 cm^{-1}, which is assigned to CH_2 side chain vibrations of collagen that can be used to monitor collagen integrity[21,29]. An increase in this ratio indicates the decrease in quality of collagen in the system together with a decrease in collagen integrity[21]. There was an increase in A_{1542}/A_{1340} ratio in 1 H post-L group ($p < 0.001$), indicating the decrease in collagen quality, whereas the ratio was observed to be decreased in 3H post-L group ($p < 0.001$) in comparison to that of 1 H post-L group (Fig. 3h). This finding implicated that the quality of collagen gradually increases over time.

The secondary structure of proteins in experimental groups were analyzed via comparing peak intensities in the second derivative spectra in 1700–1600 cm^{-1} spectral region[21] (Fig. 4). The results were presented in Table 4, and significant alterations in protein secondary structure were observed. The decreased intensities of peaks corresponding to antiparallel β-sheet (1681 cm^{-1}) and α-helical (1659 cm^{-1})[21,42] structures in 1 H post-L group were observed to be increased significantly in 3 H post-L group ($p < 0.001$) in comparison to 1 H post-L group. A similar alteration was observed in peak intensities of native β-sheet structures (1637 cm^{-1})[21], but the alterations were not statistically significant. Moreover, the peak intensities of aggregated β-sheet structure (1628 cm^{-1})[21] were slightly increased in 1 H post-L group and was significantly decreased in 3 H post-L group ($p < 0.05$) when compared to 1 H post-L group.

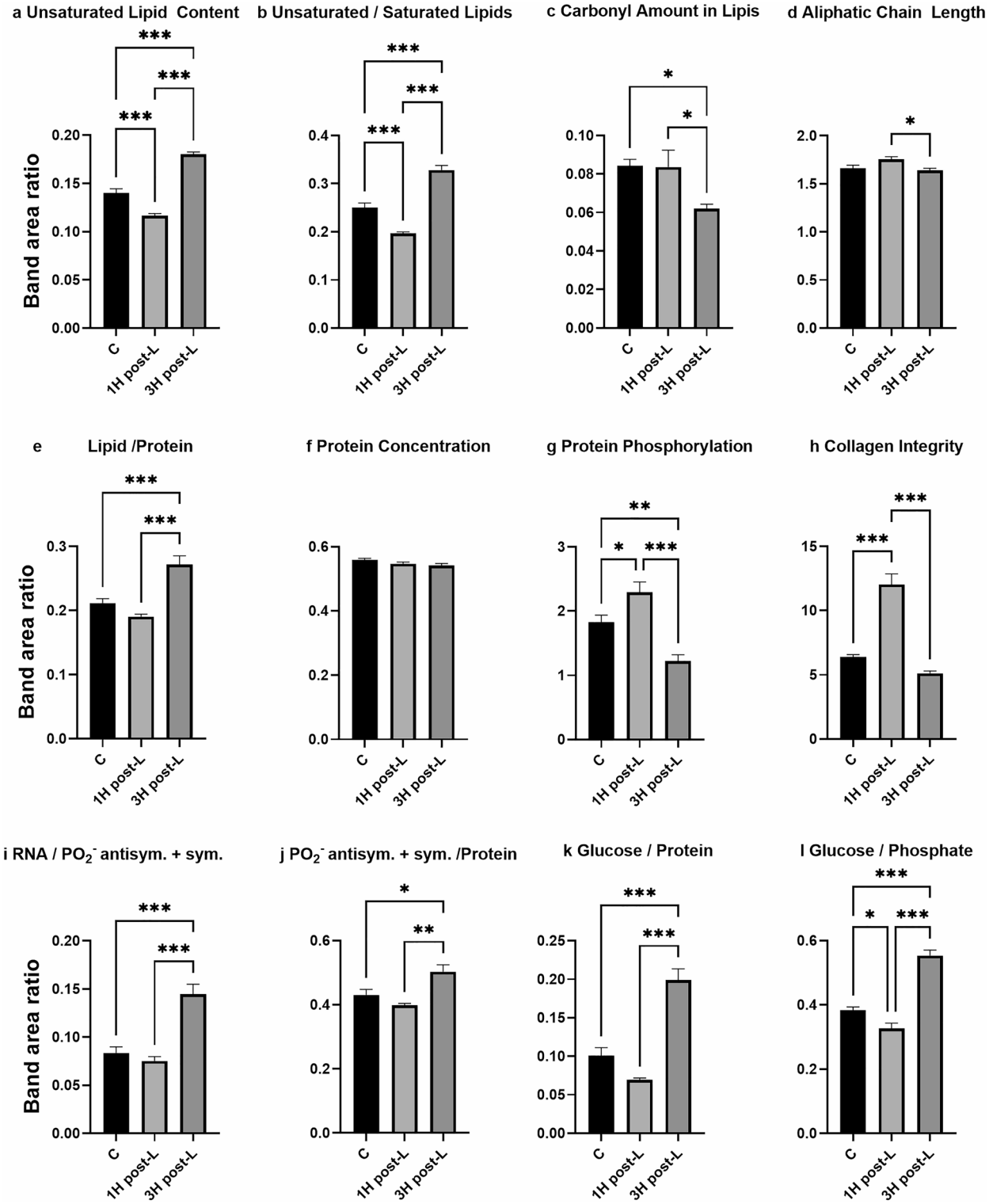

Fig. 3. The bar graphs demonstrating the alterations in band area ratios of (a) Unsaturated lipid content, (b) Unsaturated/saturated lipids, (c) Carbonyl amount in lipids, (d) Aliphatic chain length, (e) Lipid/protein, (f) Protein concentration, (g) Protein phosphorylation, (h) Collagen integrity, (i) RNA/PO^{2-} antisym. + sym. stretching, (j) PO^{2-} antisym. + sym. stretching/protein, (k) Glucose/protein, (l) Glucose/phosphate for control 1 H post-L and 3 H post-L groups. The data was analyzed via one-way ANOVA with Tukey's test as a post-hoc test. The degree of significance was denoted as $^{*}p < 0.05$, $^{**}p < 0.01$, $^{***}p < 0.001$.

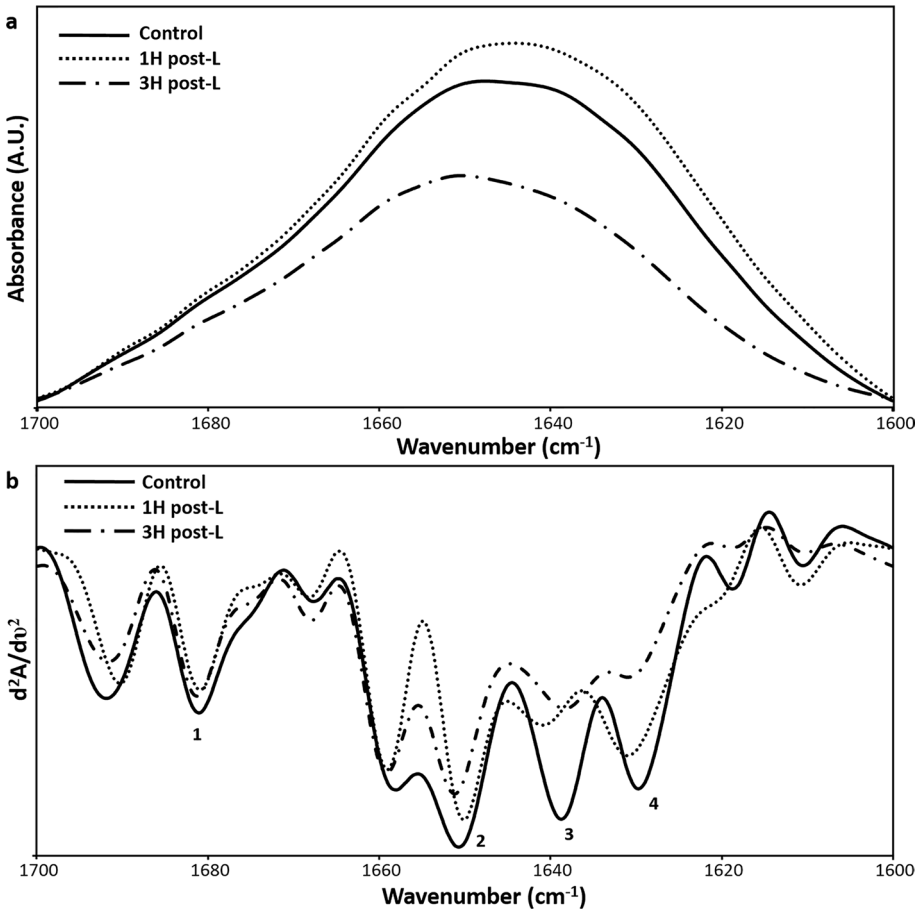

Fig. 4. The representative absorbance (a) and second derivative (b) spectra of control, 1 H post-L and 3 H post-L groups in 1700–1600 cm^{-1} region. The investigated protein secondary structural sub-bands under amide I band were labelled in the figure with numbers [1: antiparallel β-sheet structure; 2: α-helical structure; 3: native β-sheet structure; and 4: aggregated β-sheet structure].

Functional Groups	Control	1 H post-L	3 H post-L
Antiparallel β-sheet structure (at 1681 cm^{-1})	−0.091 ± 0.008	−0.049 ± 0.003**	−0.110 ± 0.011‡‡‡
α-helical structure (at 1659 cm^{-1})	−0.159 ± 0.015	−0.113 ± 0.007*	−0.202 ± 0.007*, ‡‡‡
Native β-sheet structure (at 1637 cm^{-1})	−0.121 ± 0.019	−0.115 ± 0.006	−0.128 ± 0.019
Aggregated β-sheet structure (at 1628 cm^{-1})	−0.117 ± 0.010	−0.137 ± 0.013	−0.095 ± 0.006‡

Table 4. Alterations in the intensities of main functional groups in the second derivative FTIR data in 1700–1600 cm^{-1} region of FTIR spectra representing the alterations in protein secondary structure for ADSCs in control, 1 H post-L and 3 H post-L groups. The data were represented as mean ± standard error of mean. Comparison was performed by the one-way ANOVA test with Tukey's as a post-hoc test. A p value equal or less than 0.05 was considered as statistically significant (*$p < 0.05$, **$p < 0.01$, ***$p < 0.001$). The degree of significance was denoted by * for the comparison of control with the other groups, by ‡ for the comparison of 1 H post-L group with 3 H post-L group.

Nucleic acids and carbohydrates

The most apparent differences in between 1 H and 3 H post-L groups were noted in the 1250–850 cm^{-1} region of the FTIR spectra (Fig. 2d). The bands located at 1236 and 1079 cm^{-1} are assigned to the PO_2^- antisymmetric and symmetric stretching vibrations, respectively, which both have contributions from nucleic acids and phospholipids[21,24,28,32,33,43]. As previously mentioned, the sub-band located at 970 cm^{-1} can be easily distinguished in the spectra of 1 H post-L group. Moreover, the sub-bands located at 1035 cm^{-1}, which originates from the C-O stretching vibrations of carbohydrates and glucose[26,28,33], and 990 cm^{-1}, which is assigned to RNA backbone vibrations[33,39,40,44], were clearly noticed in the spectra of 3 H post-L group (Fig. 2d). The band areas of these sub-bands were significantly increased in 3 H post-L group (Table 2).

The ratio of band areas of 990 cm^{-1} to the sum of the PO_2^- antisymmetric and symmetric stretching band areas ($A_{990}/A_{1236+1079}$) was used to monitor RNA content[33] in the ADSCs. This ratio was observed to be significantly increased in 3 H post-L group ($p < 0.001$, Fig. 3i). This finding indicated that RNA and therefore protein synthesis was amplified at 3-hour post-irradiation, which will later on result in an increased protein content. Moreover, the PO_2^- antisymmetric + symmetric/protein ratio ($A_{1236+1079}/A_{1643+1542}$)[33], which was calculated by the use of relevant band areas (Table 3), was observed to be significantly increased in 3 H post-L group ($p < 0.001$, Fig. 3j). This finding also indicated that the nucleic acid or phospholipid content was significantly amplified at 3-hour post-irradiation.

In order to more precisely comment on the utilization of carbohydrate resources in ADSCs, glucose/protein ($A_{1035}/A_{1643+1542}$) and glucose/phosphate (A_{1035}/A_{1079}) band area ratios were calculated[26,33,45,46] (Table 3). These ratios were observed to be decreased at 1 H post-L group and significantly increased in 3 H post-L group, which revealed a significantly decreased utilization of carbohydrate sources in 3 H post-L group ($p < 0.001$, Fig. 3k and l). This was further supported by the increase in the glucose or carbohydrate band located at 1035 cm^{-1} in the spectra of 3 H post-L group (Fig. 2).

Discussion

The application of red or infrared spectrum in photobiomodulation may lead to inconstant outcomes in cellular processes or "hormesis" in cells, due to the biphasic dose response observed in this optical window[16,17]. Furthermore, photobiomodulation has been reported to give rise to differential outcomes such as stimulating physiological processes or inhibiting the progression of a pathological condition[8,47], where the exact molecular mechanism is yet to be resolved. Accordingly, this spectral characterization study aimed to assess the short-term outcomes of photobiomodulation on composition, structure and function of biomolecules in ADSCs subjected to 671 nm low-level laser irradiation, utilizing FTIR spectroscopy. The results revealed apparent differences in the FTIR spectra at 1-hour and 3-hour post-irradiation. Upon low-level laser exposure at 671 nm, short-term alterations were observed over time in protein secondary structure, protein phosphorylation, lipid composition, metabolic turnover of carbohydrate sources, membrane structure and function with a temporary lateral phase separation in ADSCs.

In a cell, the content, composition and distribution of proteins and lipids, such as level of unsaturation, aliphatic chain length, membrane thickness etc., are crucial parameters for the structural and functional association of molecules, and are strongly connected to ion channel and membrane function[20]. Exposure to 671 nm laser irradiation at a fluency of 25 J/cm^2 resulted in temporary alterations in lipid composition and structure in ADSCs. Mainly, the unsaturated lipid amount and the ratio of unsaturated/saturated lipids were significantly decreased at 1-hour post-irradiation, and were significantly increased after three hours. The content of carbonyl-ester group containing lipids remained unchanged at 1-hour post-irradiation, however, was significantly decreased after three hours. Moreover, the aliphatic chain length of lipids was slightly increased at 1-hour post-irradiation, and were significantly decreased at 3-hour post-irradiation. These findings indicate a change in lipid composition and distribution as a response to laser irradiation over time, which may lead to an irregularity in the distribution of lipids between the inner and outer leaflets of the bilayer, which refers to membrane asymmetry[27]. The variations in membrane asymmetry together with alterations in membrane thickness may in turn disturb membrane function, as structural organization of lipids and proteins may influence ion channel functioning and membrane potential[20,48].

Lipid order is a structural parameter that reflects the organization and flexibility of individual acyl chains in lipids[33]. In contrast, membrane fluidity is a dynamic parameter that measures the mobility of lipid components, such as lateral diffusion. An increase in membrane order typically leads to enhanced membrane rigidity, while an increase in membrane fluidity is generally accompanied by a decrease in order, indicating greater acyl chain flexibility[21]. One hour after laser exposure, we observed an increase in order, demonstrated by a shift to lower wavenumber values of the CH_2 antisymmetric stretching vibration, along with an increased fluidity, indicated by the increase in bandwidth of this peak. This inconsistency had been reported to designate the presence of lateral phase separation within the membrane structure[21]. Phase separation or domain formation is one of the physical phenomena resulting from the dynamic organization of the lipid bilayer. Not only lipids, but also proteins that are embedded or attached to membranes can be laterally arranged within a phase separated membrane according to the lipid-protein interactions[49,50]. One such example for the formation of immiscible domains are membrane rafts, which are liquid-ordered patches in membranes with an increased thickness compared to the surrounding and faster dynamics. Another important factor is that living cell membranes are in a thermodynamic non-equilibrium and constantly undergoes lipid turnover, membrane trafficking, etc[51]. Recently, Shen et al.[51]. have studied phase behavior of endoplasmic reticulum (ER) via stimulated Raman scattering microscopy in live cells, and reported that metabolism of saturated fatty acids, having high phase transition temperatures and longer fatty acyl chain lengths, led to solid-like domain formation in the ER. However, metabolism of unsaturated fatty acids, having lower phase transition temperatures, did not form membrane domains[51]. Therefore, lipid composition in membrane structure could be a determining factor for the observed lateral phase separation. Our results have also shown the altered lipid composition, a slightly increased aliphatic chain length at 1-hour post-irradiation together with a temporary lateral phase separation in membranes. However, at 3-hour post-irradiation, this separation was terminated with a decreased order accompanied by an increased membrane fluidity, along with a significant decrease in aliphatic chain length of lipids.

Membrane fluidity not only influences the permeability of the membrane, but the structure and function of membrane proteins are also sensitive to the composition, order and fluidity of lipid environments[49,52]. In addition to the observed increase in membrane order and fluidity one hour after irradiation, we noted changes in protein secondary structure, including a decrease in α-helical and antiparallel β-sheet structures along with a slight increase in aggregated β-sheet structures. Furthermore, at one-hour post-irradiation, the quality of collagen

molecules appeared to decline while protein phosphorylation showed a significant increase (Fig. 3). Besides, a distinct peak located at 970 cm^{-1}, which is attributed to phosphorylated proteins and nucleic acids[23,38–40], was easily noticed in the FTIR spectra at one-hour post-irradiation. These alterations were observed to be reversed at 3-hour post-irradiation. Photobiomodulation was previously reported to lead to alterations in phosphorylation of some specific proteins that aid in cell survival[16,53,54].

Heat shock proteins (HSPs) are responsible of modulation of cellular homeostasis and their expression levels increase in stress conditions. Although low-level laser irradiation in photobiomodulation delivers low energy and does not result in an increase in heat in the exposed samples, photobiomodulation induces changes in cellular metabolism and ROS production in a small scale acting as a mild stressor, which is suggested to result in an increased viability and survival[55]. Exposure to 660 nm light emitting diode at 50 W/cm^2 for 15, 30 and 60 min was reported to enhance Hsp expression in human fibroblasts[56]. A pre-exposure to 810 nm diode laser at fluencies of 34.27 J/cm^2 and 44.88 J/cm^2 was reported to promote cytoprotection in rat retina by resulting in an elevated Hsp70 expression and a reduction in the expression level of cleaved caspase-3[57]. Our results indicated a slightly decreased Hsp70 protein expression level at 1-hour post-irradiation, which was elevated at 3-hour post-irradiation (Fig. 1d and e). This non-significant increase in Hsp70 protein expression level after 3 h may be a result of the protein phosphorylation and structural alterations observed at 1-hour post-irradiation, as Hsp70 was reported to play a role in protein repair[56]. Furthermore, studies have reported that alterations in membrane lipid composition, microheterogeneity and especially fluidity can trigger stress signaling responses through altered lipid-protein interactions and the formation of microdomains can modulate Hsp protein expression level[49,58]. Our finding of slightly increased Hsp70 protein expression level may be a consequence of the altered membrane lipid composition, order and fluidity. Future work is needed to confirm the relation in between photobiomodulation-induced membrane stress and heat shock response.

The metabolic turnover of carbohydrate resources in a cell can be monitored by the use of glucose/phosphate (A_{1035}/A_{1079}) and glucose/protein ($A_{1035}/A_{1643+1542}$) band area ratios in an FTIR spectrum[26,45,46]. An increase in the ratios implies the accumulation of carbohydrate resources, therefore a decreased metabolic turnover or activity. The results revealed a decreased metabolic activity at 3-hour post-irradiation, whereas at 1-hour post-irradiation, the metabolic turnover of the carbohydrate sources were more pronounced. This decreased utilization of carbohydrate resources may indicate the decrease in oxidative phosphorylation at 3-hour post-irradiation. Photobiomodulation via the use of red or near infrared light was reported to activate cytochrome c oxidase, a member of the mitochondrial respiratory chain[16,47]. Supporting our findings, Wang et al.[47] have reported that photobiomodulation with 660 nm light resulted in a more pronounced ATP production in human ADSCs at lower doses (3 J/cm^2), while higher doses (30 J/cm^2) led to a progressively lower ATP production 3 h after irradiation. In addition, the mitochondrial membrane potential of human ADSCs was reported to be significantly increased with respect to control 1-hour after photobiomodulation with 660 nm light at 3 J/cm^2[47].

The data presented collectively reveals the short-term alterations in composition, structure and function of biomolecules in ADSCs exposed to 671 nm photobiomodulation. This study is first to report the spectral characterization of the initial response of ADSCs exposed to photobiomodulation. However, there are some limitations of the study. This current study could be regarded as a preliminary work, as the effects of continuous low-level laser irradiation only at 671 nm at a fixed dose was considered. In addition, the study only concentrated to alterations at 1-hour and 3-hour post-irradiation. Therefore, how varying doses or different time intervals might affect the stated alterations needs further exploration. Furthermore, the sample size is relatively limited. It should be noted that this current study has been mainly focused on the spectral characterization of structural, compositional and dynamic alterations in biomolecules induced by photobiomodulation, and the expression level of only one protein was assessed. Future exploration related to the modulation of molecular signaling pathways by low-level laser irradiation, such as pathways associated with cell survival, proliferation and phosphorylated protein response, is crucial in order to confirm and justify the presented results.

Conclusion

This study comprehensively examined the short-term compositional and structural alterations induced by photobiomodulation on ADSCs using FTIR spectroscopy. Photobiomodulation initially triggered an immediate stress response, and over time it led to significant changes in lipid composition, protein phosphorylation and protein secondary structure, membrane order and dynamics with a temporary lateral phase separation, and alterations in utilization of carbohydrate sources in ADSCs. These findings may further implicate the activation of cellular adaptation mechanisms in ADSCs upon exposure to low-level laser irradiation, leading to the increased viability or "hormesis" in cells. The outcomes of the current study are further valuable in providing new insights into the mechanism of action of photobiomodulation and enhancing the understanding of its therapeutic potential for future applications.

Methods

Cell culture

This study is performed in accordance with relevant guidelines and regulations. All methods are reported in accordance with ARRIVE guidelines. In this current study, we have used the ADSCs that were isolated from an adult male Wistar-albino rat originating from the same primary source as reported in our earlier work[59]. The applied procedures for ADSC isolation were approved by the Ethics Committee of Aydın Adnan Menderes University (approval number 64583101/2017/087), and the use of archived ADSCs previously isolated and characterized[59] was also approved by the Ethics Committee of Aydın Adnan Menderes University (approval number 64583101/2024/59). The ADSCs were transferred into flasks containing cell culture media (α-MEM + 5% L-glutamine). The cells were cultured in media supplemented with 5% Penicillin-Streptomycin and 10%

FBS (Sigma-Aldrich, ABD) and incubated at 37 °C with 5% CO_2, with media changes occurring every three days. Once the cells reached 80% confluence, they were passaged into new flasks. Following the isolation and expansion at the third passage, the ADSCs were divided into three study groups: a control group, a group that underwent low-level laser irradiation and was harvested one-hour post-irradiation (1 H post-L), and a group that was irradiated and harvested three hours' post-irradiation (3 H post-L).

Low-level laser irradiation

After characterization, third-passage cells were plated in a 24-well plate at a density of 1×10^5 cells per well. The next day, each well was exposed to a 671 nm wavelength laser (MRL-FN-671, Thorlabs, China), with the laser output recorded at 243 mW at the experimental setup, as shown in Fig. 1b.

In order to identify most suitable dose of laser irradiation to observe the cellular responses, cells were irradiated with laser fluences at 1, 5, 10, 25, and 50 J/cm². This effective fluence range of 1–50 J/cm² was selected based on the literature that apply photobiomodulation on mesenchymal stem cells[4,60,61]. To achieve target fluences of 1, 5, 10, 25, and 50 J/cm², irradiation times were calculated using the formula D = P × t/A, where D is the desired fluence (J/cm2), P is the laser output (W), t is the exposure time (seconds), and A is the irradiated area (cm²), which corresponds approximately to the well surface area (1.9 cm² per well in a 24-well plate). Initially, cells were exposed to these different fluences to identify the most effective dose for promoting proliferation at 24 hours' post-irradiation. In order to assess this, MTT test was applied. Cells were plated in 24-well plates at a density of 5×10^4 cells per well using DMEM. After 24 h of incubation, the medium was replaced with serum-free and phenol red-free DMEM. The wells were then irradiated with a 671 nm laser at doses of 1, 5, 10, 25, or 50 J/cm² for varying durations. Following irradiation, the complete cell medium was added, and the cells were incubated for an additional 24 h. The next day, the cells were treated with DMEM containing 0.5 mg/mL MTT for 2 hours. The resulting formazan crystals were dissolved in 500 µL of DMSO, and the absorbance was measured at 457 nm using a plate reader.

Based on these findings, the fluence that exhibited the most significant biological effect was chosen for further investigation. Subsequently, to evaluate the short-term cellular responses to photobiomodulation, cells were irradiated with the selected fluence, and analyses were conducted at 1 h and 3 h following irradiation. The experiments were repeated twice, in each repetition three different wells were used and scanned as separate samples. For each experimental replicate, all groups were seeded and grown in a single 24-well plate, with one row of three wells designated as control, the subsequent row as 1 H post-L, and the other row as 3 H post-L groups. Therefore, in each experimental group, there were a total of 6 biological replicates of ADSCs that were investigated via FTIR spectroscopy.

Determination of Hsp70 protein expression level

Determination of the protein expression levels were performed as described previously[62]. ADSCs were lysed in RIPA lysis buffer (Merck Millipore, Darmstadt, Germany) containing a 1:10 protease inhibitor cocktail (Sigma-Aldrich, USA) and then centrifuged at 15,000 g for 10 min at 4 °C. The supernatants were combined with a sample buffer that included 0.5 M Tris-HCl (pH 6.8), glycerol, 10% SDS, bromophenol blue, and β-mercaptoethanol, and then boiled at 95 °C for 5 min. The protein concentration in the lysates was measured using a bicinchoninic acid protein assay kit (ThermoFisher Scientific, USA). An equal amount of protein (20 µg) from each group in triplicates was loaded onto a polyacrylamide gel (with 4% stacking and 12% resolving gels), subjected to gel electrophoresis, and transferred to a polyvinylidene fluoride membrane (Millipore, Bedford, MA, USA). After blocking, the membrane was incubated overnight at 4 °C with primary antibodies against Hsp70 (1:1000, Bioss, USA) and GAPDH (1:5000, Bioss, USA), followed by washing. The secondary antibody (1:2000 anti-mouse IgG HRP, Abcam, UK) was then applied at room temperature for 2 h, and ECL substrate (BIO-RAD, California, USA) was added after washing. Finally, the membrane was visualized using the UVP system (LAB Denmark APS, Denmark) with a consistent exposure time of 5 min. Protein band intensities were quantified using ImageJ (MD, USA, 64-bit version) software.

ATR-FTIR spectroscopic data collection and data analysis

FTIR spectra of ADSCs subjected to photobiomodulation at different time intervals (control, 1 H and 3 H post-irradiation) was collected by Perkin Elmer Spectrum-Two FTIR spectrometer (Perkin Elmer, USA) coupled with an attenuated total reflection (ATR) unit containing a diamond crystal (Perkin Elmer, USA). ADSCs were trypsinized, collected and washed twice with HBSS to prevent environmental contamination, and finally were re-suspended in HBSS at 2×10^6 cells/ml. Then, the cells were centrifuged at 1200 rpm for 3 min to remove the supernatant. Finally, the resultant cell suspension was placed on the ATR diamond crystal surface and dried under mild nitrogen flow at room temperature for 10 min to remove excess water. The spectra were collected within the spectral range of 4000–450 cm^{-1}; 100 scans were collected for each interferogram at a resolution of 2 cm^{-1}. A background scan was taken prior to the experiment, in order to prevent the interference of atmospheric water vapor and carbon dioxide. The spectra of three replicates from each sample was collected, all of which yielded similar spectra, and their average was used for data analysis. The collection of spectral data and their analysis was performed via Perkin Elmer Spectrum software (version 10.5.2, Perkin Elmer, USA). Band areas were calculated, and band positions were determined based on the center of weight at 75% of peak height, confirmed through the second derivatives of the peaks. The bandwidth values of specific absorption peaks were measured as the width corresponding to 75% band intensity. Spectra were baseline corrected and normalized relative to the Amide A band located at 3282 cm^{-1} for visual demonstration.

In order to determine the intensities associated with different protein secondary structures, the band intensities in second derivative spectra in 1700–1600 cm^{-1} region was analyzed using OPUS 8.5 software (Bruker Optik GmbH, Germany). The second derivative spectra were generated using a 9- point Savitzky-Golay

smoothing algorithm. Subsequently, the spectra were vector normalized in the 1700–1600 cm^{-1} region, and the corresponding peak intensities at the minima were calculated by OPUS 8.5 software.

Statistical analysis

Data were expressed as mean ± standard error of mean. Statistical analysis was performed using the GraphPad Prism 10.5.0 software (La Jolla, CA, USA). First, the data was analyzed via Anderson Darling normality test, which revealed that data follow a normal distribution. Therefore, statistical analysis was performed via one-way ANOVA together with Tukey's test applied as a post-hoc test. The results of MTT and Hsp70 protein expression levels were also evaluated via one-way ANOVA with Dunn's test as a post-hoc test. A p value of less than 0.05 was considered as statistically significant. The degree of significance of the post-hoc test was denoted by * for the comparison of control with the other groups, by ‡ for the comparison of 1 H post-L group with 3 H post-L group ($^{*}p < 0.05$, $^{**}p < 0.01$, $^{***}p < 0.001$).

Data Availability

The datasets generated in the current study are available from the corresponding author on request.

Data availability

The datasets generated in the current study are available from the corresponding author on request.

Received: 15 May 2025; Accepted: 6 August 2025
Published online: 23 August 2025

References

1. Atala, A. Advances in tissue and organ replacement. *Curr. Stem Cell. Res. Ther.* **3** (1), 21–31 (2008).
2. Galipeau, J. & Sensébé, L. Mesenchymal stromal cells: clinical challenges and therapeutic opportunities. *Cell. Stem Cell.* **22** (6), 824–833 (2018).
3. Dahbour, S. et al. Mesenchymal stem cells and conditioned media in the treatment of multiple sclerosis patients: clinical, ophthalmological and radiological assessments of safety and efficacy. *CNS Neurosci. Ther.* **23** (11), 866–874 (2017).
4. Chang, S. Y., Carpena, N. T., Kang, B. J. & Lee, M. Y. Effects of photobiomodulation on stem cells important for regenerative medicine. *Med. Lasers*. **9** (2), 134–141 (2020).
5. AlGhamdi, K. M., Kumar, A. & Moussa, N. A. Low-level laser therapy: a useful technique for enhancing the proliferation of various cultured cells. *Lasers Med. Sci.* **27** (1), 237–249 (2012).
6. Migliario, M., Sabbatini, M., Mortellaro, C. & Renò, F. Near infrared low-level laser therapy and cell proliferation: the emerging role of redox sensitive signal transduction pathways. *J. Biophotonics*. **11** (11), e201800025. https://doi.org/10.1002/jbio.201800025 (2018).
7. Zecha, J. A. E. M. et al. Low level laser therapy/photobiomodulation in the management of side effects of chemoradiation therapy in head and neck cancer: part 1: mechanisms of action, dosimetric, and safety considerations. *Suppor Care Cancer*. **24** (6), 2781–2792 (2016).
8. Liu, S. et al. Low-level laser selectively inhibiting colorectal cancer cell metabolic activity and inducing apoptosis for delaying the development of intestinal cancer. *Photochem. Photobiol Sci.* **22**, 1707–1720 (2023).
9. Feng, J. et al. Photobiomodulation with 808-nm diode laser enhances gingival wound healing by promoting migration of human gingival mesenchymal stem cells via ROS/JNK/NF-κB/MMP-1 pathway. *Lasers Med. Sci.* **35**, 1831–1839 (2020).
10. Amini, A. et al. Stereological and molecular studies on the combined effects of photobiomodulation and human bone marrow mesenchymal stem cell conditioned medium on wound healing in diabetic rats. *J. Photochem Photobiol B*. **182**, 42–51 (2018).
11. de Andrade, A. L. M. et al. Photobiomodulation effect on the proliferation of adipose tissue mesenchymal stem cells. *Lasers Med. Sci.* **34** (4), 677–683 (2019).
12. Yin, K., Zhu, R., Wang, S. & Zhao, R. C. Low level laser (LLL) attenuate LPS-induced inflammatory responses in mesenchymal stem cells via the suppression of NF-kappaB signaling pathway in vitro. *PLoS One*. **12** (6), e0179175. https://doi.org/10.1371/journal.pone.0179175 (2017).
13. Yin, K., Zhu, R., Wang, S. & Zhao, R. C. Low-Level laser effect on proliferation, migration, and antiapoptosis of mesenchymal stem cells. *Stem Cells Dev.* **26** (10), 762–775 (2017).
14. Taylor, D. N., Winfield, T. & Wynd, S. Low-level laser light therapy dosage variables vs treatment efficacy of neuromusculoskeletal conditions: A scoping review. *J. Chiropr. Med.* **19** (2), 119–127 (2020).
15. Moore, P., Ridgway, T. D., Higbee, R. G., Howard, E. W. & Lucroy, M. D. Effect of wavelength on low-intensity laser irradiationstimulated cell proliferation in vitro. *Lasers Surg. Med.* **36**, 8–12 (2005).
16. Hamblin, M. R. Mechanisms and mitochondrial redox signaling in photobiomodulation. *Photochem. Photobiol.* **94** (2), 199–212 (2018).
17. Huang, Y. Y., Sharma, S. K., Carroll, J. & Hamblin, M. R. Biphasic dose response in low level light therapy - an update. *Dose Response*. **9** (4), 602–618 (2011).
18. Avci, P. et al. Low-level laser (light) therapy (LLLT) in skin: stimulating, healing, restoring. *Semin Cutan. Med. Surg.* **32** (1), 41–52 (2013).
19. Mamalis, A., Siegel, D. & Jagdeo, J. Visible red light emitting diode photobiomodulation for skin fibrosis: key molecular pathways. *Curr. Derm Rep.* **5**, 121–128 (2016).
20. Awayda, M. S., Shao, W., Guo, F., Zeidel, M. & Hill, W. G. ENaC-membrane interactions: regulation of channel activity by membrane order. *J. Gen. Physiol.* **123** (6), 709–727 (2004).
21. Bozkurt, O., Severcan, M. & Severcan, F. Diabetes induces compositional, structural and functional alterations on rat skeletal soleus muscle revealed by FTIR spectroscopy: a comparative study with EDL muscle. *Analyst* **135** (12), 3110–3119 (2010).
22. Vileno, B. et al. Evidence of lipid peroxidation and protein phosphorylation in cells upon oxidative stress photo-generated by fullerols. *Biophys. Chem.* **152** (1–3), 164–169 (2010).
23. Chen, L. et al. Synchrotron infrared measurements of protein phosphorylation in living single PC12 cells during neuronal differentiation. *Anal. Chem.* **84** (9), 4118–4125 (2012).
24. Aksoy, C., Kaya, F. A., Kuşkonmaz, B. B., Uçkan, D. & Severcan, F. Structural investigation of donor age effect on human bone marrow mesenchymal stem cells: FTIR spectroscopy and imaging. *Age (Dordr)*. **36** (4), 9691. https://doi.org/10.1007/s11357-014-9691-7 (2014).
25. Aksoy, C., Guliyev, A., Kilic, E., Uckan, D. & Severcan, F. Bone marrow mesenchymal stem cells in patients with beta thalassemia major: molecular analysis with attenuated total reflection-Fourier transform infrared spectroscopy study as a novel method. *Stem Cells Dev.* **21** (11), 2000–2011 (2012).

26. Sen, I. et al. Lipid profiles of adipose and muscle tissues in mouse models of juvenile onset of obesity without high fat diet induction: a fourier transform infrared (FT-IR) spectroscopic study. *Appl. Spectrosc.* **69** (6), 679–688 (2015).
27. Cakmak, G., Severcan, M., Zorlu, F. & Severcan, F. Structural and functional damages of whole body ionizing radiation on rat brain homogenate membranes and protective effect of amifostine. *Int. J. Radiat. Biol.* **92** (12), 837–848 (2016).
28. Abbas, S. et al. Diagnosis of malignant pleural mesothelioma from pleural fluid by fourier transform-infrared spectroscopy coupled with chemometrics. *J. Biomed. Opt.* **23** (10), 1–14 (2018).
29. Mata-Miranda, M. M. et al. Biochemical similarity between cultured chondrocytes and in situ chondrocytes by chemometric analysis from FTIR microspectroscopy. *Biotechnol. Rep. (Amst).* **24**, e00391. https://doi.org/10.1016/j.btre.2019.e00391 (2019).
30. Ravera, F., Efeoglu, E. & Byrne, H. J. Vibrational spectroscopy for in vitro monitoring stem cell differentiation. *Molecules* **25** (23), 5554. https://doi.org/10.3390/molecules25235554 (2020).
31. Ezer Özer, N. & Mollaoğlu, D. Changes in secondary structure of protein in skeletal muscle due to high-carbohydrate or high-fat diets. *Meandros Med. Dent. J.* **26** (1), 1–11 (2025).
32. Dogan, A., Severcan, F., Tuzlaci, A. & Guvenc, B. H. Comparison of human breast milk vs commercial formula-induced early trophic enteral nutrition during postoperative prolonged starvation in an animal model. *Sci. Rep.* **14** (1), 21610. https://doi.org/10.1038/s41598-024-67863-4 (2024).
33. Severcan, F. et al. Decoding myasthenia gravis: advanced diagnosis with infrared spectroscopy and machine learning. *Sci. Rep.* **14** (1), 19316. https://doi.org/10.1038/s41598-024-66501-3 (2024).
34. Lee, B. S., Lin, C. P., Hung, Y. L. & Lan, W. H. Structural changes of er:yag laser-irradiated human dentin. *Photomed. Laser Surg.* **22** (4), 330–334 (2004).
35. Aljdaimi, A., Devlin, H., Dickinson, M. & Alfutimie, A. Effect of 2.94 μm er: YAG laser on the chemical composition of hard tissues. *Microsc Res. Tech.* **81** (8), 887–896 (2018).
36. Vieira, W. F. et al. Vibrational spectroscopy of muscular tissue intoxicated by snake venom and exposed to photobiomodulation therapy. *Lasers Med. Sci.* **33** (3), 503–512 (2018).
37. Magrini, T. D., dos Santos, N. V., Milazzotto, M. P., Cerchiaro, G. & da Silva Martinho, H. Low-level laser therapy on MCF-7 cells: a micro-Fourier transform infrared spectroscopy study. *J. Biomed. Opt.* **17** (10), 101516. https://doi.org/10.1117/1.JBO.17.10.101516 (2012).
38. Staniszewska, E., Malek, K. & Baranska, M. Rapid approach to analyze biochemical variation in rat organs by ATR FTIR spectroscopy. *Spectrochim Acta Mol. Biomol. Spectrosc.* **118**, 981–986 (2014).
39. Maziak, D. E. et al. Fourier-transform infrared spectroscopic study of characteristic molecular structure in cancer cells of esophagus: an exploratory study. *Cancer Detect. Prev.* **31** (3), 244–253 (2007).
40. Talari, A. C. S., Martinez, M. A. G., Movasaghi, Z., Rehman, S. & Rehman I. U. Advances in fourier transform infrared (FTIR) spectroscopy of biological tissues. *App Spec. Rev.* **52** (5), 456–506 (2016).
41. Lucke, L. D. et al. Low-level laser and adipose-derived stem cells altered remodelling genes expression and improved collagen reorganization during tendon repair. *Cell. Prolif.* **52** (3), e12580. https://doi.org/10.1111/cpr.12580 (2019).
42. Garip, S. et al. Structural effects of Simvastatin on liver rat [corrected] tissue: fourier transform infrared and Raman microspectroscopic studies. *J. Biomed. Opt.* **21** (2), 25008. https://doi.org/10.1117/1.JBO.21.2.025008 (2016).
43. Bozkurt, O. et al. Structural alterations in rat liver proteins due to streptozotocin-induced diabetes and the recovery effect of selenium: fourier transform infrared microspectroscopy and neural network study. *J. Biomed. Opt.* **17** (7), 076023. https://doi.org/10.1117/1.JBO.17.7.076023 (2012).
44. Ozdil, B., Güler, G., Acikgoz, E., Kocaturk, D. C. & Aktug, H. The effect of extracellular matrix on the differentiation of mouse embryonic stem cells. *J. Cell. Biochem.* **121** (1), 269–283 (2020).
45. Gazi, E. et al. Applications of fourier transform infrared microspectroscopy in studies of benign prostate and prostate cancer. A pilot study. *J. Pathol.* **201** (1), 99–108 (2003).
46. Gazi, E. et al. The combined application of FTIR microspectroscopy and ToF-SIMS imaging in the study of prostate cancer. *Faraday Discuss.* **126**, 41–59 (2004).
47. Wang, Y., Huang, Y. Y., Wang, Y., Lyu, P. & Hamblin, M. R. Red (660 nm) or near-infrared (810 nm) photobiomodulation stimulates, while blue (415 nm), green (540 nm) light inhibits proliferation in human adipose-derived stem cells. *Sci. Rep.* **7** (1), 7781. https://doi.org/10.1038/s41598-017-07525-w (2017).
48. Turker, S., Ilbay, G., Severcan, M. & Severcan, F. Investigation of compositional, structural, and dynamical changes of pentylenetetrazol-induced seizures on a rat brain by FT-IR spectroscopy. *Anal. Chem.* **86** (3), 1395–1403 (2014).
49. Escribá, P. V. et al. Membranes: a meeting point for lipids, proteins and therapies. *J. Cell. Mol. Med.* **12** (3), 829–875 (2008).
50. Shimokawa, N. & Hamada, T. Physical concept to explain the regulation of lipid membrane phase separation under isothermal conditions. *Life (Basel).* **13** (5), 1105. https://doi.org/10.3390/life13051105 (2023).
51. Shen, Y. et al. Metabolic activity induces membrane phase separation in Endoplasmic reticulum. *Proc. Natl. Acad. Sci. USA.* **114** (51), 13394–13399 (2017).
52. Portaccio, M., Faramarzi, B. & Lepore, M. Probing biochemical differences in lipid components of human cells by means of ATR-FTIR spectroscopy. *Biophysica* **3** (3), 524–538 (2023).
53. Liebert, A. D., Bicknell, B. T. & Adams, R. D. Protein conformational modulation by photons: a mechanism for laser treatment effects. *Med. Hypotheses.* **82** (3), 275–281 (2014).
54. Chu, Y. H., Chen, S. Y., Hsieh, Y. L., Teng, Y. H. & Cheng, Y. J. Low-level laser therapy prevents endothelial cells from TNF-alpha/cycloheximide-induced apoptosis. *Lasers Med. Sci.* **33** (2), 279–286 (2018).
55. Cardoso, F. D. S., Barrett, D. W., Wade, Z., Gomes da Silva, S. & Gonzalez-Lima, F. Photobiomodulation of cytochrome c oxidase by chronic transcranial laser in young and aged brains. *Front. Neurosci.* **16**, 818005. https://doi.org/10.3389/fnins.2022.818005 (2022).
56. Choi, S. H. et al. Light-emitting diode irradiation using 660 Nm promotes human fibroblast HSP90 expression and changes cellular activity and morphology. *J. Biophotonics.* **12** (9), e201900063. https://doi.org/10.1002/jbio.201900063 (2019).
57. Sun, Y., Zhang, S., Liao, H., Wang, J. & Wang, L. Pre-exposure to low-power diode laser irradiation promotes cytoprotection in the rat retina. *Lasers Med. Sci.* **30**, 127–133 (2015).
58. Nagy, E. et al. Hyperfluidization-coupled membrane microdomain reorganization is linked to activation of the heat shock response in a murine melanoma cell line. *Proc. Natl. Acad. Sci. USA.* **104**, 7945–7950 (2007).
59. Kilic, M. A., Abdulova, A., Tanriverdi, G. & Bilgin, M. D. Evaluation of combined effects of brief electrical stimulation and Schwann-like cells on sciatic nerve injury model. *Bioelectromagnetics* **44** (7–8), 192–203 (2023).
60. de Lima, R. D. N. et al. Low-level laser therapy alleviates the deleterious effect of doxorubicin on rat adipose tissue-derived mesenchymal stem cells. *J. Photochem. Photobiol B.* **196**, 111512. https://doi.org/10.1016/j.jphotobiol.2019.111512 (2019).
61. Shi, Z., Li, S., Chen, W. & Yan, H. The effect of blue and green light on human umbilical cord mesenchymal stem cells for promoting proliferation and wound healing. *Sci. Rep.* **15** (1), 14787. https://doi.org/10.1038/s41598-025-99083-9 (2025).
62. Bilir-Yildiz, B., Sunay, F. B., Yilmaz, H. F. & Bozkurt-Girit, O. Low-intensity low-frequency pulsed ultrasound ameliorates sciatic nerve dysfunction in a rat model of cisplatin-induced peripheral neuropathy. *Sci. Rep.* **12** (1), 8125. https://doi.org/10.1038/s41598-022-11978-z (2022).

Acknowledgements

The authors would like to thank to Prof. Mehmet Dincer Bilgin for their help and support throughout the study.

In addition, the authors are grateful to Prof. Dr. Murat Uygun for their help and support regarding the use of the FTIR spectrophotometer.

Author contributions

O.B.G. and M.A.K. designed the study. M.A.K. carried out the isolation of ADSCs and cell culture experiments, O.B.G. and M.A.K. performed FTIR spectroscopic data collection. O.B.G. analyzed and interpreted the spectroscopic data. O.B.G. and M.A.K. prepared the final manuscript. All authors have revised and approved the final version of the manuscript.

Funding

This study was partly supported by the Aydın Adnan Menderes University Scientific Research Fund (grant number TPF-21034).

Declarations

Competing interests

The authors declare no competing interests.

Additional information

Supplementary Information The online version contains supplementary material available at https://doi.org/10.1038/s41598-025-15190-7.

Correspondence and requests for materials should be addressed to O.B.-G.

Reprints and permissions information is available at www.nature.com/reprints.

Publisher's note Springer Nature remains neutral with regard to jurisdictional claims in published maps and institutional affiliations.